

Single-Stage, Single-Switch Input-Current-Shaping Technique with Reduced Switching Loss

Laszlo Huber and Milan M. Jovanović

Delta Products Corporation
Power Electronics Laboratory
P.O. Box 12173
5101 Davis Drive
Research Triangle Park, NC 27709

Abstract - In this paper, a new single-stage, single-switch input-current-shaping (S⁴ICS) technique which features substantially reduced turn-on switching loss of the switch in a S⁴ICS flyback topology is described. In the proposed technique, the turn-on switching loss due to the discharging of the output capacitance of the switch is reduced by turning on the switch when its voltage is minimum. To achieve the turn-on loss reduction for a wide range of line and load conditions, the flyback transformer is continuously operated at the boundary of the continuous conduction mode (CCM) and discontinuous conduction mode (DCM) by employing a variable-frequency control. The performance of the new S⁴ICS flyback technique was evaluated on a 70-W (20-V/3.5-A) experimental prototype.

I. INTRODUCTION

Recently, a number of single-stage input-current-shaping techniques have been introduced. In a single-stage approach, input-current shaping, isolation, and high-bandwidth control are performed in a single step, i.e., without creating an intermediate dc bus. Among the single-stage circuits, a number of circuits described in [1]-[10] seem particularly attractive because they can be implemented with only one semiconductor switch and a simple control. All these single-stage, single-switch input-current shaping (S⁴ICS) circuits integrate the boost-converter front end with the forward-converter or the flyback-converter dc/dc stage. Fig. 1 shows the S⁴ICS flyback converter implementation introduced in [7]. The two additional primary windings, N_1 and N_2 , are employed to keep the voltage of energy-storage (bulk) capacitor C_B below a desired level in the entire line and load ranges (e.g., 400 V at the universal line range of 90-264 V_{rms}). Boost inductor L_B can operate either in the discontinuous conduction mode (DCM) or in the continuous conduction mode (CCM). Generally, the CCM operation offers a slightly higher efficiency compared to the DCM operation. However, the DCM operation gives a lower total harmonic distortion (THD) of the line current compared to that of the CCM operation.

One of the major contributors to losses of the S⁴ICS flyback converter in Fig. 1 is the turn-on switching loss of switch SW due to the discharging of the output capacitance (C_{oss}) of the switch. When the circuit in Fig. 1 operates at a constant switching frequency f_s with a CCM magnetizing

current of the flyback transformer, the power dissipation of the switch associated with the capacitive-discharging turn-on loss is

$$P_{ON(cap)} = C_{oss} V_{SW(off)}^2 f_s / 2, \quad (1)$$

where $V_{SW(off)} = V_B + nV_o$ is the voltage across the switch during the off-time, and $n = N_p/N_s$ is the turns ratio of the transformer. Since $V_{SW(off)}$ increases as the line voltage increases because V_B increases with the line voltage, the capacitive-discharging turn-on switching loss is maximum at high line. Generally, MOSFET switches with a lower on-resistance, $R_{DS(on)}$, which reduces the conduction loss, possess larger output capacitance C_{oss} . Therefore, at high switching frequencies, the capacitive-discharging turn-on switching loss has a detrimental effect on the efficiency of the circuit in Fig. 1, especially, at high line. Because $P_{ON(cap)}$ does not depend on the load current but only on the line voltage, $P_{ON(cap)}$ dominates the switch losses at light loads and, consequently, limits the light-load efficiency. A reduced light-load efficiency makes very difficult to comply with Environmental Protection Agency's Energy Star and similar European requirements, which set a voluntary power-consumption limit of an idling personal computer.

When the flyback transformer in Fig. 1 operates with a DCM magnetizing current, the switch voltage during the off-time after the magnetizing current decreases to zero oscillates around V_B with an amplitude equal to nV_o because of the resonance between the magnetizing inductance of the transformer and the output capacitance of the switch. Therefore, the S⁴ICS flyback converter operating with a

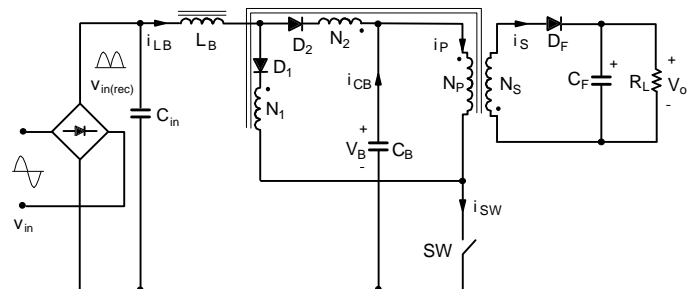


Fig. 1 S⁴ICS flyback converter introduced in [7].

DCM magnetizing current of the transformer also suffers from capacitive-discharging turn-on switching loss $P_{ON(cap)}$. The maximum $P_{ON(cap)}$ in a DCM flyback converter is the same as the $P_{ON(cap)}$ in a CCM flyback converter.

In this paper, a new S^4ICS technique which features substantially reduced turn-on switching loss of the switch in a S^4ICS flyback converter is described. In this technique, the turn-on switching loss due to the discharging of the output capacitance of the switch is reduced by turning on the switch when its voltage is minimum or close to the minimum. To achieve the turn-on loss reduction for a wide range of line and load conditions, the flyback transformer is continuously operated at the boundary of the CCM and DCM by employing a variable-frequency control. The implementation of the new S^4ICS flyback converter is described in Section II, whereas principles of operation, including topological stages and key waveforms, are provided in Section III. Finally, experimental results obtained on a 70-W (20-V/3.5-A) prototype circuit for an adapter application are given in Section IV.

II. TOPOLOGY

In the S^4ICS flyback converter in Fig. 1, two additional primary windings, N_1 and N_2 , are employed to keep the voltage of energy-storage (bulk) capacitor C_B below the desired level in the entire line and load ranges. Winding N_1 appears in series with boost inductor L_B during the on-time of switch SW, whereas winding N_2 appears in series with L_B during the off-time of the switch. By connecting the windings so that the voltage across each of them when they conduct the boost-inductor current is in opposition to the line voltage, the volt-second balance of the boost-inductor core is achieved at a substantially lower voltage of the energy-storage capacitor compared to the corresponding circuit without the windings. In addition, winding N_2 provides a path for a direct transfer of a part of the input energy to the output during the off-time of the switch. Generally, direct energy transfer improves the conversion efficiency.

The same performance of the S^4ICS converter can be achieved if windings N_1 and N_2 are implemented as portions of the primary winding of the transformer by employing tapping, as shown in Fig. 2. Both implementations of windings N_1 and N_2 require the same number of pins of the transformer. However, since the implementation in Fig. 2 does not require additional windings, the construction of the transformer in Fig. 2 is simpler than that in Fig. 1. The construction of the transformer can be further simplified by selecting $N_1 + N_2 = N_p$, because then only one tap on the primary winding is required, as shown in Fig. 3. Also, the S^4ICS flyback converter in Fig. 3 requires only one diode, D , instead of two diodes, D_1 and D_2 , in Fig. 2.

Boost inductor L_B in the S^4ICS flyback converter in Fig. 1 can operate in both DCM and CCM. For the CCM operation of L_B , it is necessary to have a substantial inductance

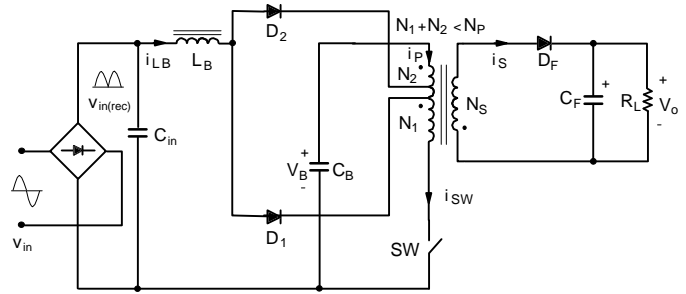


Fig.2 Implementation of S^4ICS flyback converter in Fig. 1 with double-tapped primary winding of the transformer.

connected in series with winding N_1 and/or winding N_2 , as explained in [8]. The additional inductance can either be the leakage inductance of the winding (implemented by an appropriate structure of the transformer) and/or an external inductance. In the S^4ICS flyback converter in Fig. 2, boost inductor L_B can operate also in both DCM and CCM. To achieve the CCM operation of L_B in Fig. 2, it is more convenient to employ an external inductance in series with diode D_1 and/or diode D_2 . It should be noticed that the S^4ICS flyback converter in Fig. 3 is only suitable for the DCM operation of L_B .

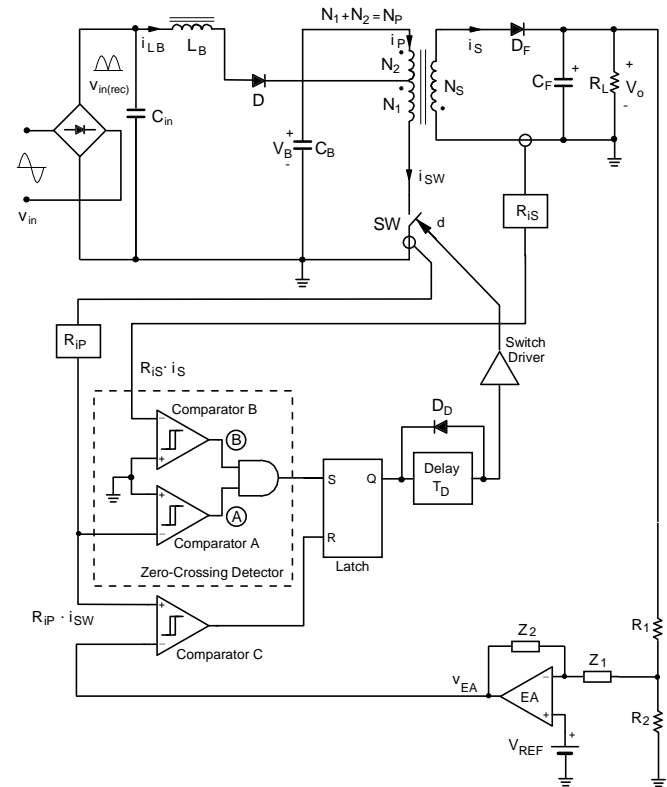


Fig. 3 Power stage and control circuit of the proposed S^4ICS flyback converter with single-tapped primary winding of the transformer.

III. PRINCIPLES OF OPERATION

Principles of operation are illustrated on the example of the S⁴ICS flyback converter in Fig. 3. To facilitate the analysis of operation, Figs. 4 and 5 show topological stages and key waveforms of the variable-frequency S⁴ICS flyback converter in Fig. 3, respectively. To simplify the analysis, it is assumed that all semiconductor components are ideal except for the output capacitance of the primary switch, C_{oss} . In addition, the flyback transformer is modeled by an ideal transformer with magnetizing inductance L_M in parallel with primary winding N_P , as shown in Fig. 4. Finally, the input voltage of the converter is considered constant during a switching cycle because the switching frequency is much larger than the line frequency.

Since boost inductor L_B in Fig. 3 operates in the DCM and the magnetizing inductance of the flyback transformer operates at the DCM/CCM boundary, at the moment immediately before switch SW is turned on, currents i_{LB} , i_M , and i_S are zero. After switch SW is closed at $t=T_0$, i_M starts flowing through the switch, as shown in Fig. 4(a). Since energy-storage capacitor voltage V_B is approximately constant during a switching cycle, magnetizing current i_M increases linearly with a slope

$$\frac{di_M}{dt} = \frac{V_B}{L_M}, \quad (2)$$

as shown in Fig. 5. If rectified line voltage $v_{in(rec)}$ is lower than $(N_1/N_P)V_B$, no boost-inductor current i_{LB} can flow because diode D is reverse biased. Otherwise, i_{LB} flows through diode D , winding N_1 , and switch SW as indicated in Fig. 4(a). The slope of i_{LB} is given by

$$\frac{di_{LB}}{dt} = \frac{v_{in(rec)} - (N_1/N_P)V_B}{L_B}. \quad (3)$$

Because of the magnetic coupling between windings N_1 and N_2 , current i_{P1} flowing through both N_1 and N_2 is

$$i_{P1} = -\frac{N_1}{N_P} i_{LB}. \quad (4)$$

Also, as can be seen from Fig. 4(a), energy-storage-capacitor current i_{CB} is

$$i_{CB} = i_M + i_{P1} = i_M - \frac{N_1}{N_P} i_{LB}. \quad (5)$$

By rewriting (5) as

$$i_M = i_{CB} + \frac{N_1}{N_P} i_{LB}, \quad (6)$$

it can be seen that during the on-time, energy from two sources is stored in the magnetic field of the flyback transformer. Namely, part of the magnetizing energy is supplied from the bulk capacitor, as in the case of the conventional flyback converter, whereas part of the energy is supplied directly from the line. Generally, direct energy storage from the line improves the conversion efficiency.

The two components of i_M are indicated in the i_M waveform in Fig. 5.

Finally, the switch current is obtained as

$$i_{SW} = i_{CB} + i_{LB} = i_M + \left(1 - \frac{N_1}{N_P}\right) i_{LB}. \quad (7)$$

As can be seen in Fig. 3, during the on-time, the output of comparator A in the zero-crossing-detector circuit is low, whereas the output of comparator B is high. Consequently, the output of the AND gate is low, holding the set (S) input of the SR latch low during the entire on-time.

The on-time of the switch is terminated at $t=T_1$ when sensed voltage $R_{ip}i_{SW}$ at the input of comparator C reaches the level of control voltage v_{EA} . At that moment the reset (R) input of the latch changes from low level to high level, forcing the latch output Q to change from high to low. Because diode D_D is connected in parallel to the delay circuit, the high-to-low transition of Q is immediately transferred to the input of the switch driver, i.e., switch SW is turned off without a delay.

After switch SW is turned off, currents i_{LB} and i_{CB} continue to flow through output capacitance C_{oss} of the switch, as shown in Fig. 4(b), and switch voltage v_{SW} starts increasing. When switch voltage v_{SW} reaches $V_B + nV_o$ at $t=T_2$, secondary-side rectifier D_F becomes forward biased, as shown in Fig. 4(c). Because of the conduction of rectifier D_F , switch voltage v_{SW} stays clamped to $V_B + nV_o$. At the same time, reflected magnetizing current $(N_P/N_S)i_M = -(N_P/N_S)i_{P1}$ starts flowing on the secondary side. In addition, at $t=T_2$, boost-inductor current i_{LB} begins flowing through diode D , winding N_2 , and energy-storage capacitor C_B , as shown in Fig. 4(c). Because of the magnetic coupling between winding N_2 and secondary winding N_S , i_{LB} is also reflected to the secondary. According to Fig. 4(c), the secondary current is given by

$$i_S = \frac{N_P}{N_S} i_M + \frac{N_2}{N_S} i_{LB}. \quad (8)$$

As can be seen from (8), i_S , which during the off-time supplies energy to the output, is composed of two components which draw energy from two different sources. The energy of the component associated with the magnetizing current is obtained from the energy stored in the magnetic field during the on-time, while the energy associated with the boost-inductor current is drawn directly from the input line. The two i_S components are indicated in the i_{LB} waveform in Fig. 5. Generally, direct energy transfer from the line to the output improves the conversion efficiency.

It should be noticed that at $t=T_2$ the outputs of comparators A and B in the zero-crossing-detector circuit in Fig. 3 change states. Namely, the output of comparator A changes from low to high, whereas the output of comparator B changes from high to low. These changes do not have any effect on the output of the AND gate, i.e., the S input of the latch, which continues to stay low. However, at $t=T_2$, the R input of the

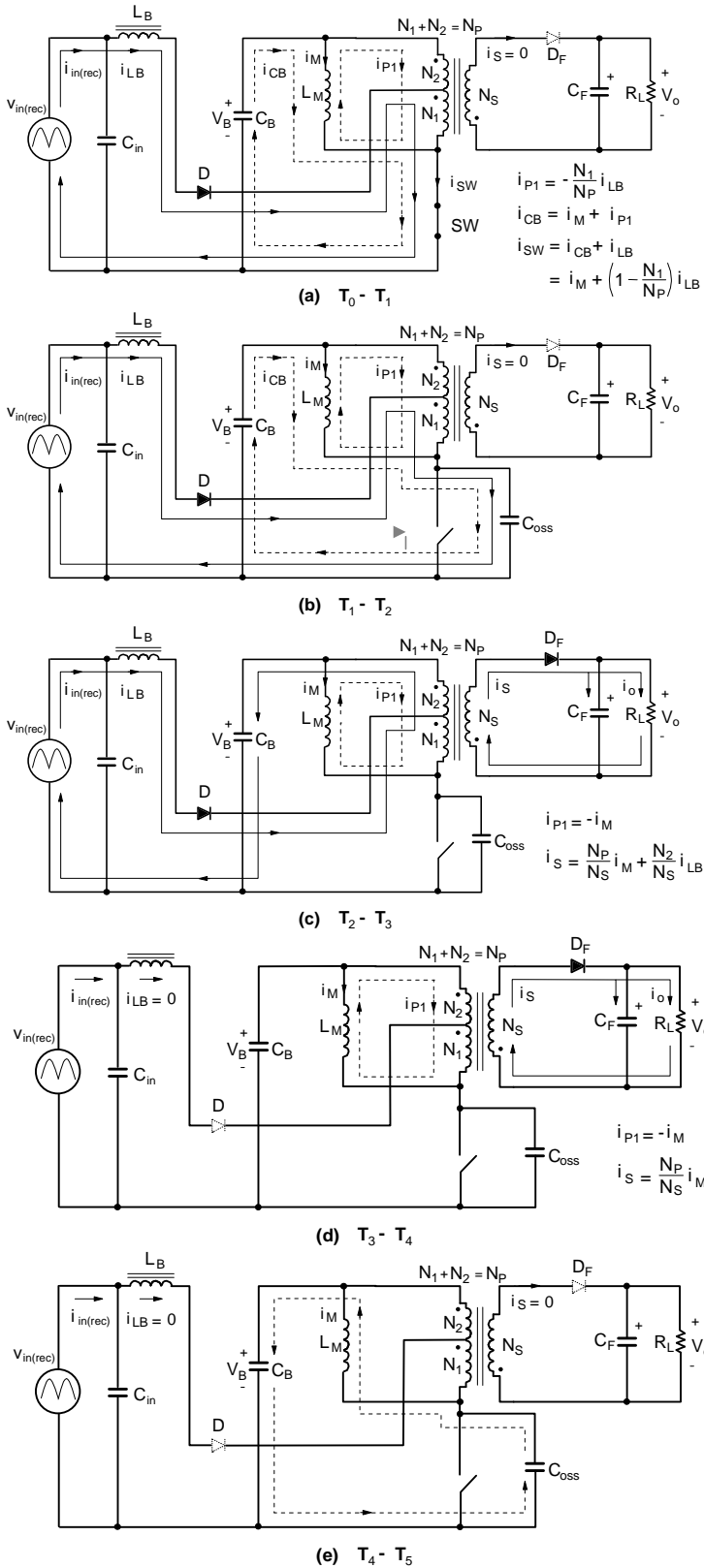


Fig. 4 Topological stages of the S^4ICS flyback converter in Fig. 3.

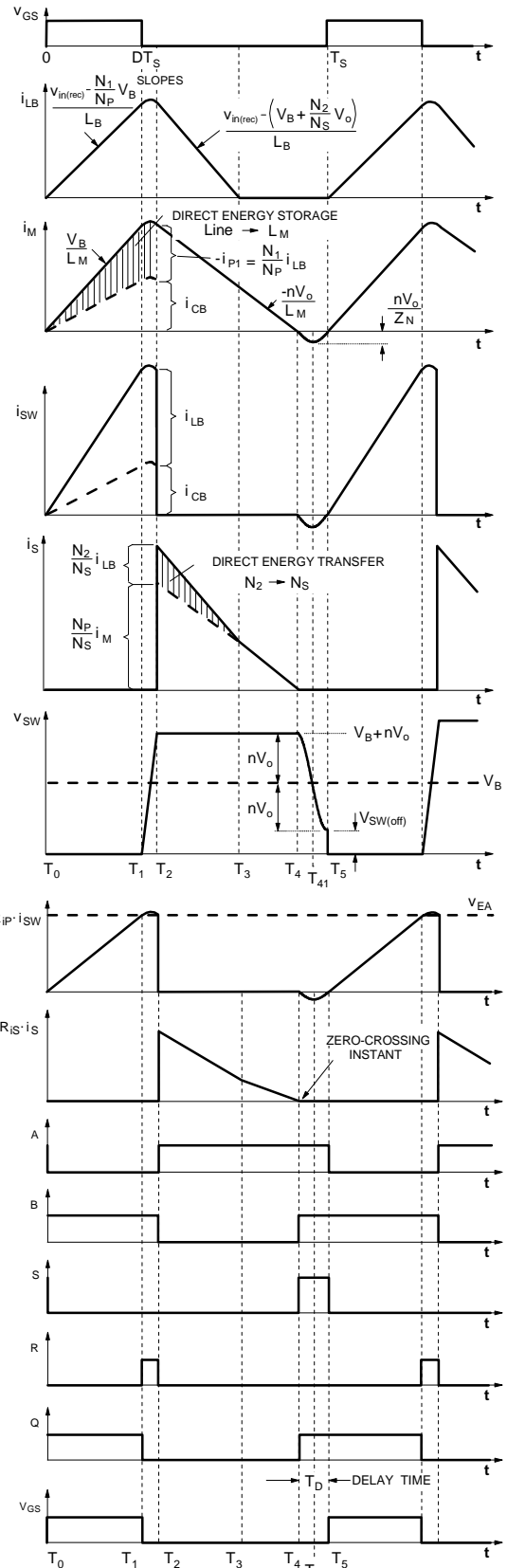


Fig. 5 Key waveforms of the S^4ICS flyback converter in Fig. 3.

latch changes state from high to low because the primary current stops flowing and sensed voltage $R_{ip}i_{SW}$ becomes zero. Since the SR latch is only triggered with positive edge transitions, the high-to-low transition at the R input does not change the state of the latch, i.e., output Q stays low keeping switch SW off.

It should be also noticed that at $t=T_2$, the instantaneous, simultaneous transitions of the outputs of comparators A and B in the opposite directions create a signal-racing situation. This may generate a false pulse at the AND-gate output that may false trigger the latch. This racing situation in Fig. 5 is the result of the assumption that the leakage inductances of the transformer are negligible so that switch current i_{SW} and secondary current i_s commute instantaneously. However, in a practical circuit, due to the leakage inductances of the transformer, the commutation of the currents takes a short but finite time. In fact, in the presence of the leakage inductances, the output of comparator B changes from high to low at $t=T_2$, which marks the beginning of the commutation period, whereas the output of comparator A changes state at the end of the commutation period, which occurs at a later instant. Therefore, in the presence of the leakage inductances of the transformer, the signal racing at $t=T_2$ does not exist, and no false triggering of the latch can occur.

As can be seen from Fig. 5, after $t=T_2$, currents i_{LB} and i_M decrease linearly. According to Fig. 4(c), the downslope of i_{LB} is given by

$$\frac{di_{LB}}{dt} = -\frac{V_B + (N_2/N_S)V_o - v_{in(rec)}}{L_B}, \quad (9)$$

whereas the downslope of i_M is given by

$$\frac{di_M}{dt} = -\frac{nV_o}{L_M}. \quad (10)$$

From (9), it can be seen that winding N_2 reduces energy-storage-capacitor voltage V_B required to reset L_B for the amount of the induced voltage $(N_2/N_S)V_o$ across winding N_2 .

When at $t=T_3$, i_{LB} decreases to zero, diode D turns off, as shown in Fig. 4(d). However, the linearly decreasing magnetizing current $(N_p/N_S)i_M = -(N_p/N_S)i_{P1}$ continues to flow in the secondary until it becomes zero at $t=T_4$ (Fig. 5).

To operate the flyback converter at the DCM/CCM boundary, primary switch SW needs to be turned on immediately after i_s falls to zero at $t=T_4$. However, if switch SW is turned on at $t=T_4$, capacitive-discharging turn-on loss $P_{ON(cap)}$ would not be reduced because switch SW would be turned on with voltage $V_{SW(off)} = V_B + nV_o$ across it. To achieve a reduction of $P_{ON(cap)}$, it is necessary to delay the turn-on of primary switch SW with respect to the instant at which secondary current i_s falls to zero. This can be achieved by inserting a delay circuit between the output of the SR latch and the switch driver, as shown in Fig. 3. When i_s becomes zero at $t=T_4$, the output of comparator B in the zero-crossing detector changes from low to high, causing the output of the AND gate (S input of the latch) to go high. The low-to-high

transition at the S input of the latch causes the Q output of the latch to also change from low to high. However, because of the delay circuit, the change at the latch output appears at the input of the switch driver after a constant delay T_D . This delay is determined so that switch SW is turned on with the minimum voltage across it.

As shown in Fig. 4(e), when switch SW is kept off after $t=T_4$, magnetizing inductance L_M of the transformer and output capacitance C_{oss} of the switch form a series resonant circuit. During the resonance, switch voltage v_{SW} decreases and reaches a minimum of

$$V_{SW(off),min} = V_B - nV_o. \quad (11)$$

at $t=T_5$. Therefore, to turn switch SW on with a minimum voltage across it, the required delay time of the controller is equal to one-half of a resonant period of the L_M - C_{oss} resonant circuit, i.e.,

$$T_D = \pi\sqrt{L_M C_{oss}}. \quad (12)$$

However, it should be noted that C_{oss} is dependent on the voltage (nonlinear capacitance), and that both L_M and C_{oss} are temperature dependent. Therefore, the constant delay calculated from (12) does not ensure that switch SW is turned on at the minimum voltage under all operating conditions. Nevertheless, the switch would be turned on close to the minimum voltage since the variations of the parameters in (12) are not large.

Finally, when switch SW is turned on at $t=T_5$ by the delayed transition at the S input of the SR latch, the output of comparator A changes from high to low causing the output of the AND gate (S input of the latch) to go low.

Since the control circuit in Fig. 3 does not have a clock to initiate a switching transition, but the turn-on and turn-off switching instants are determined by comparisons of sensed primary and secondary currents with the zero reference level, the controller works with a variable switching frequency. Moreover, both the on-time and the off-time are variable. The frequency is maximum at the highest line voltage and the minimum load, whereas the minimum switching frequency occurs at the lowest line voltage and the full load.

Switch SW can be turned on with zero voltage if the circuit is designed so that $nV_o \geq V_B$. To achieve zero-voltage switching (ZVS) in the entire line range, the ZVS condition must be met at the highest line voltage, when $V_B = V_{Bmax}$, which results in a maximum switch voltage of $V_{SWmax} \geq 2V_{Bmax}$. In universal-line (90-264 V_{rms}) applications, where a typical value of V_{Bmax} is around 400 V, a design which achieves ZVS in the entire line range would require a switch with a voltage rating in excess of 800 V. Since higher voltage-rated switches have higher on-resistance and are more expensive than their counterparts with lower voltage ratings, a design with ZVS in the entire line range neither gives the optimal performance nor it is cost effective. In fact, in a design with the optimum trade-off between performance and cost, nV_o is selected based on the desirable maximum

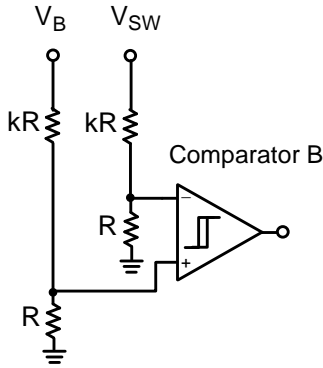


Fig. 6 Implementation of comparator *B* by sensing the primary voltage.

stress of the switch with a lower voltage (e.g., 600 V) rating. However, for such a selection of nV_o , no ZVS is achieved at high line and, very often, it is not achieved even at low line. Still, the switch is turned on with a substantially reduced voltage, resulting in a significantly lower capacitive-discharging turn-on switching loss.

The circuit in Fig. 3 can be implemented in a number of different ways. For example, the onset of the DCM can be detected by sensing the primary or secondary voltage of the transformer instead of sensing the secondary current. As an illustration, Fig. 6 shows the implementation of comparator *B* in the circuit in Fig. 3 by sensing the primary voltage, i.e., the difference between bulk voltage V_B and switch voltage v_{SW} to detect the beginning of the DCM. With this implementation of comparator *B*, the onset of the DCM is sensed by detecting the time instant $t=T_{41}$ in Fig. 5 when switch voltage v_{SW} falls below V_B . As can be seen from the v_{SW} waveform in Fig. 5, to achieve the minimum turn-on loss in this implementation of comparator *B*, the delay of the controller needs to be one

half of that in Fig. 3, which is given in (12).

Finally, it should be noticed that in some applications, the conversion efficiency of the flyback S^4 ICS can be improved by replacing secondary-side rectifier D_F in Fig. 3 by a synchronous rectifier, i.e., very low on-resistance MOSFET [11].

IV. EXPERIMENTAL RESULTS

To verify the operation and performance of the new S^4 ICS technique, a 70-W (20-V/3.5-A), universal line voltage (90-264 V_{rms}) S^4 ICS flyback converter shown in Fig. 3 with comparator *B* shown in Fig. 6 was built for an adapter application. The following components were used in the implementation of the circuit: C_{in} - 220 nF/ 250 Vac, L_B - 180 μ H, D - BYM26C, C_B - 180 μ F/400 V, Transformer - EER28L core with $N_P = 66$ turns, $N_S = 11$ turns, $N_1 = N_2 = 33$ turns, $L_M = 520$ μ H, SW - SPPX1N60S5 (600 V, 20 A, 0.19 Ω), D_F - 16CTQ100, C_F - 3x470 μ F/25 V. The control circuit was implemented using the variable-frequency power-factor-controller integrated circuit MC34262. Measured full-load line-voltage and line-current waveforms at the nominal low line ($V_{in} = 100 V_{rms}$) and the nominal high line ($V_{in} = 230 V_{rms}$) are shown in Fig. 7. The measured individual line-current harmonics were well below the IEC1000-3-2 Class-D limits, i.e., they exhibited more than 20% margin at both the nominal low line and high line. Table I summarizes the measured full-load power-factor (PF), total-harmonic-distortion (THD), bulk-capacitor-voltage (V_B), efficiency, that includes electromagnetic interference (EMI) filter and in-rush current limiter losses, and switching-frequency range. As can be seen from Table I, the maximum bulk-capacitor voltage is well below 400 V. The minimum efficiency, which occurs at low line, is above 84%.

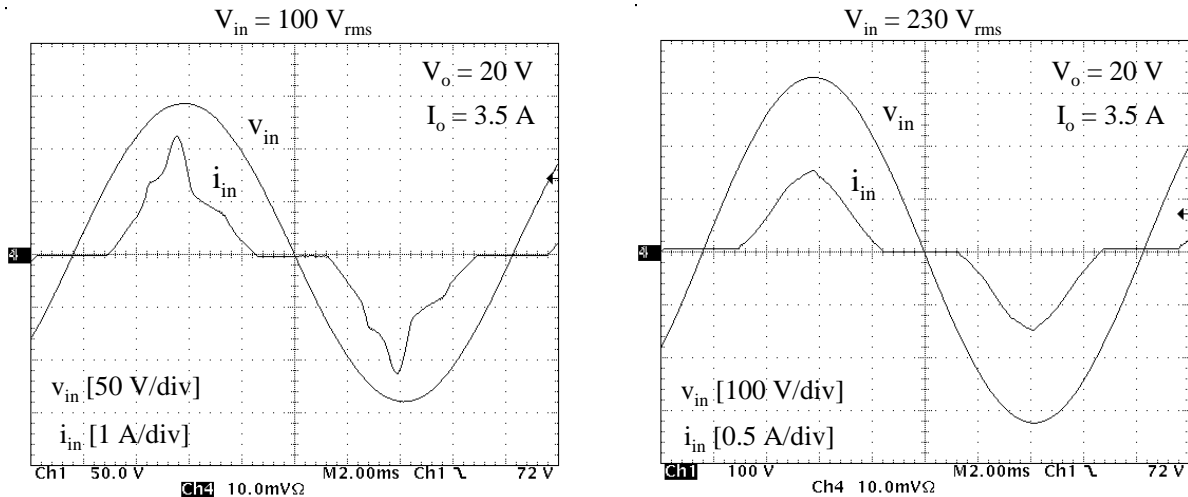


Fig. 7 Experimental line-voltage and line-current waveforms.

TABLE I
MEASURED PF, THD, V_B , EFFICIENCY, AND
SWITCHING FREQUENCY AT FULL LOAD

V_{in} [V _{rms}]	PF	THD [%]	V_B [V]	η [%]	f_s [kHz]
90	0.884	51.4	120	84.2	41-71
100	0.886	51.5	134	84.9	45-79
132	0.902	47.0	180	86.9	59-96
180	0.908	45.7	250	87.8	73-106
230	0.903	47.0	325	87.9	85-116
264	0.896	48.6	378	87.7	91-120

V. CONCLUSION

A new single-stage, single-switch input-current-shaping (S^4 ICS) technique which features substantially reduced turn-on switching loss of the switch in a S^4 ICS flyback converter is proposed. The turn-on switching loss due to the discharging of the output capacitance of the switch is reduced by turning on the switch when its voltage is minimum or close to minimum. To achieve the turn-on loss reduction for a wide range of line and load conditions, the flyback transformer is continuously operated at the boundary of the discontinuous and continuous conduction modes (DCM/CCM) by employing a variable-frequency control. The wide-bandwidth, variable-frequency control is implemented by detecting the onset of the DCM/CCM boundary and, subsequently, turning on the switch with an appropriate delay when the switch voltage becomes minimum. Because of the flyback converter topology, the proposed technique is most suitable for universal-line (90-264 V_{rms}) applications with higher output voltages and lower output currents. Due to the DCM/CCM boundary operation, the maximum energy-storage-capacitor voltage in the proposed technique is well below 400 V.

REFERENCES

- [1] M. Madigan, R. Erickson, and E. Ismail, "Integrated high-quality rectifier-regulators," *IEEE Power Electronics Specialists' Conf. (PESC) Record*, pp. 1043-1051, Jun. 1992.
- [2] S. Teramoto, M. Sekine, and R. Saito, "High power factor ac/dc converter," U.S. Patent No. 5,301,095, Apr. 5, 1994.
- [3] R. Redl and L. Balogh, "Design consideration for single-stage isolated power-factor-corrected supplies with fast regulation of the output voltage," *IEEE Applied Power Electronics Conference (APEC) Proc.*, pp.454-458, Mar. 1995.
- [4] H. Watanabe, Y. Kobayashi, Y. Sekine, M. Morikawa, and T. Ishii, "The suppressing harmonic currents, MS (magnetic switch) power supply," *IEEE International Telecommunication Energy Conf. (INTELEC) Proc.*, pp. 783-790, Oct. 1995.
- [5] F.S. Tsai, P. Markowski, and E. Whitcomb, "Off-line flyback converter with input harmonic current correction," *IEEE International Telecommunication Energy Conf. (INTELEC) Proc.*, pp. 120-124, Oct. 1996.
- [6] J. Qian and F.C. Lee, "A high efficient single stage single switch high power factor ac/dc converter with universal input," *IEEE Applied Power Electronics Conference (APEC) Proc.*, pp. 281-287, Feb. 1997.
- [7] L. Huber and M. M. Jovanović, "Single-stage, single-switch isolated power-supply technique with input-current shaping and fast output-voltage regulation," *IEEE Applied Power Electronics Conference (APEC) Proc.*, pp.272-280, Feb. 1997.
- [8] L. Huber and M. M. Jovanović, "Design optimization of single-stage, single-switch input-current shapers," *IEEE Power Electronics Specialists Conference (PESC) Rec.*, pp. 519-526, Jun. 1997.
- [9] J. Sebastian, M.M. Hernando, P. Villegas, J. Diaz, and A. Fontan, "Input current shaper based on the series connection of a voltage source and a loss-free resistor," *IEEE Applied Power Electronics Conference (APEC) Proc.*, pp. 461-467, Feb. 1998.
- [10] G. Hua, "Consolidated soft-switching ac/dc converters," U.S. Patent No. 5,790,389, Aug. 4, 1998.
- [11] M.T. Zhang, M.M. Jovanovic, and F.C. Lee, "Design considerations and performance evaluations of synchronous rectification in flyback converters," *IEEE Applied Power Electronics Conference (APEC) Proc.*, pp. 623-630, Feb. 1997.